Journal of the Indian Society of Remote Sensing (September 2018) 46(9):1353–1364
https://doi.org/10.1007/s12524-018-0779-x

RESEARCH ARTICLE

Evidence of Possible Recharge Zones for Lake Salda (Turkey)

Hüseyin Çaldırak[1] · Bedri Kurtuluş[1]

Received: 3 October 2016 / Accepted: 3 June 2018 / Published online: 16 June 2018

Abstract

This study explores the evidence of recharge locations using hydrogeochemical and physicochemical measurements in an alkaline lake, Lake Salda, in Burdur, Turkey. In-situ measurements have been performed using a conductivity–temperature–depth device to map the physicochemical dynamic of the lake. Water and sediment samples were collected on the surface and floor of the lake. A seismic study was also carried out in order to observe the geometry of the lake floor. In addition, thermal distribution was mapped using the thermal band of Landsat 7 ETM+ and Landsat 8 satellite images. Temperature and specific conductance measurements were mapped using a new technique, Empirical Bayesian Kriging (EBK), from the lake's surface to the floor. According to interpolation maps obtained from the EBK, possible water inputs were observed close to a fault at the south-eastern part of the lake. The results of thermal band imaging also reveal the probability of a fault effecting the recharge on the surface. The results of water and sediment samples present a richness in Mg^{2+} and Fe^{2+} elements respectively on the floor of the lake. Finally, seismic results show some possible recharge zones on the floor of the lake, and sediment results indicate that there should be peridotite occurrence below the alluvium unit.

Keywords Empirical Bayesian Kriging · Hydrogeochemistry · Lake Salda · Landsat · Physicochemistry · Recharge

Introduction

Lakes perform an important function in nature, the maintenance of the natural environment and ecosystems with a continuous recycling and renewal process of evaporation, precipitation and runoff (Wetzel 2001), as well as supplying freshwater for human necessities such as agriculture, drinking water, industry and recreation. Unfortunately, it is difficult to understand how the recharge processes occur due to the complexity of lakes. Physicochemical properties of water: temperature, conductivity, depth, etc. give us crucial information to determine hydrodynamic properties of lake water. Chemical parameters of water are also very important in understanding its natural sources when entering the lake (Baykal et al. 1996). Nowadays, new miniaturized and high-accuracy conductivity, temperature and depth (CTD) sensors, that are portable and easy to use for the measurement of these parameters of properties, are a primary investigative tool, providing information for aquatic environments, such as oceanic circulation, and mixing, climate processes.

The most common environmental physicochemical parameters used for water are specific conductance and temperature. Specific conductance is a measure of the ability of water to conduct electricity (Crescentini et al. 2012). In general, the higher the concentration of dissolved salts in the water, the easier it is for electricity to pass through it. Surface water temperature is a key parameter in the physics of aquatic system processes, so monitoring the distribution of water temperature is fundamental to understanding the functionality of reservoirs and lakes, especially in the summer months, thermal bedding, Thermocline, can be observed (Wetzel 2001).

Geostatistics aim at providing quantitative descriptions of natural variables distributed in space and time (Chilès and Delfiner 2012). Several geostatistical techniques are widely used and compared (Canoğlu 2015), for example kriging, which works by using a semi-variogram, is

Electronic supplementary material The online version of this article (https://doi.org/10.1007/s12524-018-0779-x) contains supplementary material, which is available to authorized users.

✉ Bedri Kurtuluş
bkurtulus@mu.edu.tr

[1] Geological Engineering Department, Muğla Sıtkı Koçman University, 48000 Mentese, Mugla, Turkey

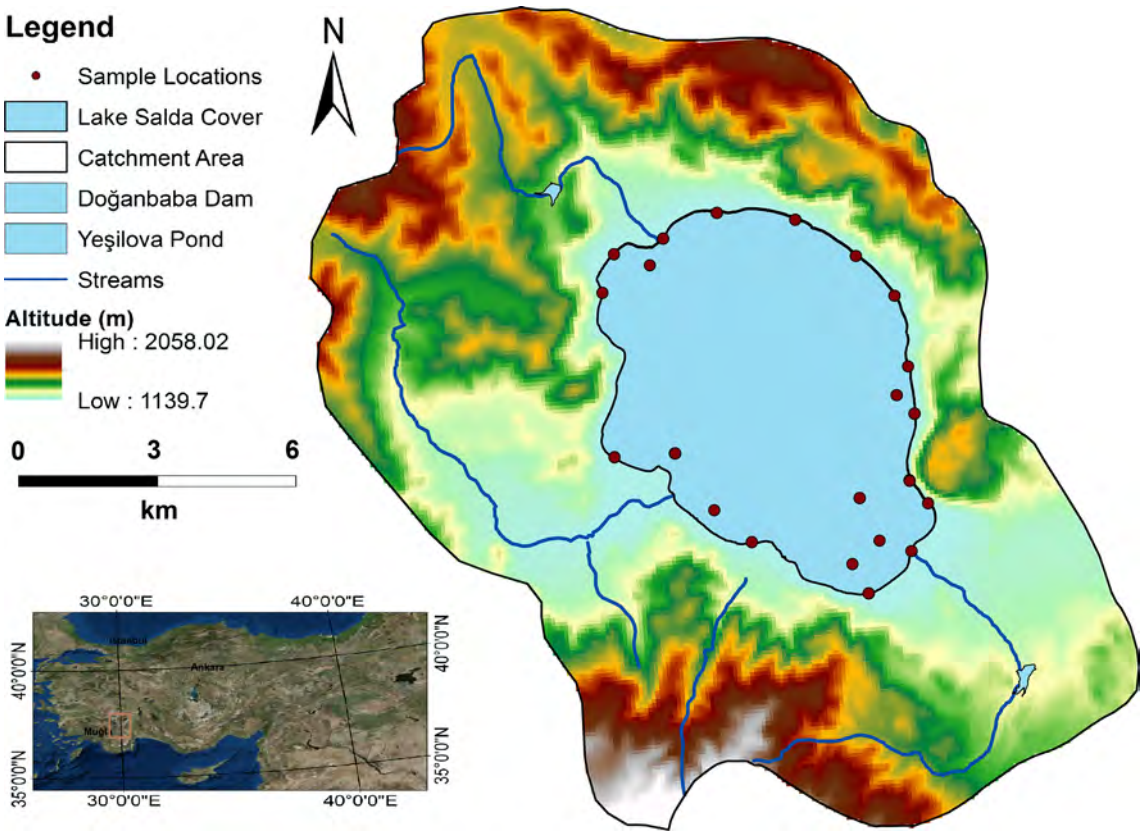

Fig. 1 Studied domain: location of study area, topographic relief map, observation points and streams

generally preferred to quantify the spatial dependence in data. In this study, a new method of Kriging is used, Emprical Bayesian Kriging. Emprical Bayesian Kriging accounts for any errors and estimates a semi-variogram model rather than a single semi-variogram (Krivoruchko 2011).

Remote sensing technology has special importance for lake management through the application of water quality monitoring (Trescott and Park 2014), and can provide useful spatio-temporal information using different band spectrums (Bonansea et al. 2015). The recent launch of the Landsat 8 satellite provides remote sensing data at high spatial resolution using the Operational Land Imager (OLI) and Thermal Infrared Sensors (TIRS). TIR band has been broadly applied to quantify Land Surface Temperature (LST) and heat (cold and hot) discharge in coastal areas (Vlassova et al. 2014).

There are over a hundred lakes in Turkey, Lake Salda being one of the largest and deepest enclosed saline lakes. The passage of cold meteoric waters through surrounding rocks occurs all over the lake (Russell et al. 1999). The stratification in Lake Salda was disrupted by water discharge from groundwater sources on the floor of the lake (Kazanci et al. 2004). Braithwaite and Zedef (1994) also suggest that the recharge of the lake could be coming from alluvial areas.

The present study focuses on determining possible recharge zones for Lake Salda using laboratory and in situ measurements with Landsat 7–8 images (thermal bands) and seismic study results. All the spatial interpolation maps were done using the Empirical Bayesian Kriging (EBK) method and its results were correlated with in situ measurements. By using spatial interpolation maps, remote sensing images and seismic profile results, evidence of possible recharge zones was presented in a conceptual model.

Study Area

Lake Salda is located in the Burdur sub-basin, in the Yesilova district. The lake is 1139 meters above sea level and covers an area of almost 45 km^2 (Fig. 1). It is known to be one of the deepest lakes in Turkey with a maximum depth of 184 m (Caldirak et al. 2017). Due to its location, it was declared an area of natural protection in 1989, and center for tourism in 2004 by the Culture and Tourism Ministries of Turkey. Lake Salda is fed by four main

streams; Zehra from the north, Karakova from the west, Köpek from the southwestern and Kuruçay stream from the southern side of the lake. The lake water is highly alkaline with pH values ranging from 8.90 to 9.05. The lake water is also rich in magnesium and is one of two important high alkaline lakes in Turkey along with Lake Van. Also, the magnesite deposits located on the west side of the lake, were related to "White Rock", which was also discovered on Mars (Russell et al. 1999).

Geological Structure

Lake Salda is located on an anticline area, and occurs in the section that lowers onto a fold axis due to the surrounding waters being collected (Altınlı 1955). It has active seismic activity and it is situated in a depression north of Mt. Eseler on the Taurus tectonic belt (Kocaefe and Ataman 1976; Kazanci et al. 2004). The geology of the area is mostly dominated by ultramafic rocks and alluvial deposits. It occurs mainly as a Quaternary Alluvial Unit and Cretaceous Marmaris Peridodite around the lake. Sarp (1976) conducted an extensive petrographical study on the peridodites, and Çapan (1980) named peridodites, Marmaris Peridotite. Marmaris Peridotite occur as serpantinized ultramafic rocks in several areas, harzburgites being more widespread than any other rock type (Sarp 1976). Besides, Middle Triassic/Lias aged Dutdere Limestone which occurred due to a tectonic effect, is another important lithological unit of the study area. It is located on the southeastern part of the lake. Dutdere Limestone occurred as medium-thick bedded, locally massif, consisting of recrystallized limestone algae in several parts of the lake, and deposited in a shallow carbonate shelf environment (Ersoy 1989). Cretaceous Dunites, exposed at the northwest, and Upper Senonian Kızılcadag Melange that is located at the southeastern part of the study area, are also important units that are shown in the drainage basin. Dunites are commonly serpentinized and contain abundant olivine and rare pyroxene crystals (Şenel et al. 1989). The age of formation is Abtian-Albian which is about 114 million years, based on K–Ar age determination (Thuizat et al. 1981). Kızılcadag melange forms serpentinite, serpentinized harzburgite, and dunite among others. It generally consists of basic volcanic rock, neritic limestone, pelagic limestone, radiolarite, chert, and dolomite block (Poisson 1977). Cretaceous Igdır Metamorphites and Jurassic/Cretaceous Orhaniye formations are rarely observed in other parts of the study area (Fig. 2).

Materials and Methods

In-Situ (CDT, Seismic Profile) Dataset and Laboratory Measurement

Using a floating platform, specific conductance, temperature and depth values were measured with the YSICastAwayTM CTD device at specified locations around the lake. The deepest measurement was taken at 96 meters depth, and was chosen on purpose for being a possible extension of the main fault, located using seismic measurements at the southwestern side of the lake. The sampling rate of the device is 3 measurements per 1 m, so the device was inserted into the water and controlled with this in mind. When the device reached the bottom of the lake, it was held for almost 20 s and then pulled back using a reel.

Specific conductance with temperature was used to identify possible recharge zones. Since conductance varies dependent on temperature, the temperature at the time of

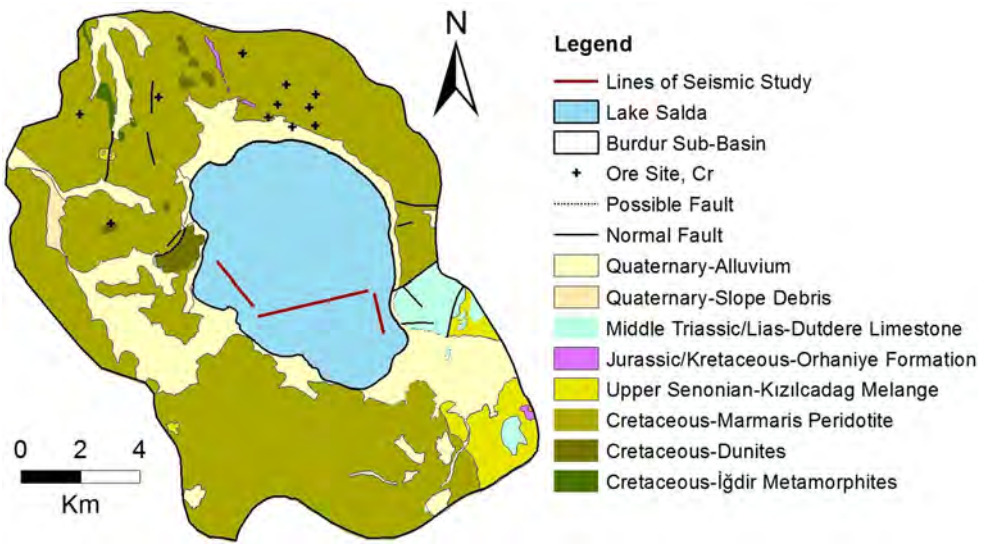

Fig. 2 Geological map of the region [modified from MTA (2010)]

the measurement becomes an essential part of the conductivity record. So, specific conductance values were taken into account for better accuracy of spatial maps beside the temperature maps.

Water and sediment samples were collected on the surface and at the lakes deepest points. Sediment core was recovered from the 96 m depth by gravity method. The water located on the top of the core, using the pressure effect in this method, was taken to analyze to determine the chemistry of the deepest water.

A seismic study was also done on specified routes to determine the floor geometry of the lake. The Innomar SES-2000 parametric sub-bottom profiler (sediment echosounder) with a frequency of 8 kHz was used.

Derivation of LST from Landsat 7 ETM+ and Landsat 8 Images

The study was carried out between 18 and 26 July 2014. Landsat 7 ETM+ and Landsat 8 satellite images were used on the dates 18 July 2014 and 26 July 2014, respectively (Table 1). The data was downloaded from United States Geological Survey's (USGS) website. For Landsat 8, band 10 and for Landsat 7 ETM+, and band 6 were used to estimate the temperature data value of each pixel in the imagery. Landsat 7 ETM+ TIR band was also corrected by filling any gaps using statistical function in Esri Arcgis. All Landsat images were rectified to a common Universal Transverse Mercator (UTM) WGS 84 coordinate system.

The methodology of converting the Digital Number (DN) of the TIRS to temperature value is done first by converting DN to Top Atmospheric Radiance (TOA) and then by using TOA values, temperature values are able to be calculated as shown in Eqs. (1) and (2). Table 2 shows the parameters needed for temperature calculations.

$$\mathrm{TOA} = \mathrm{M} \times \mathrm{DN} + \mathrm{B} \tag{1}$$

where M is the radiance multiplier. B is the radiance add. TOA is the spectral radiance in W (m^2 × ster × μm).

$$TB_{Kelvin} = \frac{K2}{Ln\left(\frac{K1}{TOA} + 1\right)} \tag{2}$$

where K1 and K2 are parameters of band specific thermal conversion constant. TB is brightness temperature in Kelvin.

The temperature values are obtained by TB are for black body. Therefore, the emissivity (ε) becomes necessary according to the nature of land cover. Land Surface Temperature could be calculated using Eq. (3) by using an average emissivity values for water (ε_{water} = 0.98) as stated in Du et al. (2015).

$$T = \frac{TB}{1 + \left(\lambda + \frac{TB}{\rho}\right) \times ln\varepsilon} \tag{3}$$

λ = wavelength of emitted radiance (λ = 11.5 um for Landsat 7, λ = 10.8 for Landsat 8 Band 10, λ = 12 for Landsat 8 Band 11) (Markham and Barker 1985). ρ = h*c/σ (1.438 × 10^{-2} m K), σ = Boltzmann constant (1.38 × 10^{-23} J/K), h = Planck's constant (6.626 × 10^{-34} J s), and c = velocity of light (2.998 × 10^8 m/s)

The temperature values are calculated in Kelvin degree. Then, the temperature values are converted into degrees Celsius by subtracting 273.15° from the Kelvin degree. All these calculations are done using ArcGIS platform (ESRI 2013).

Interpolation Method: Empirical Bayesian Kriging

Empirical Bayesian Kriging (EBK) is a new geostatistical interpolation method that automates the difficult aspects of building a valid kriging model. Other kriging methods require manual adjustments of the parameters; however,

Table 2 The metadata for (a) Landsat 8 TIR for Band 10, (b) Landsat 7 ETM+ for Band 6

	Band 10
(a) The metadata of Landsat 8 TIR	
Radiance multiplier (M)	0.0003342
Radiance add (B)	0.1
K1 (W/m^2 × ster × μm)	774.89
K2 (K)	1321.08
	Band 6
(b) The metadata of Landsat 7 ETM+ TIR VCID2	
Radiance multiplier (M)	0.037
Radiance add (B)	3.1628
K1 (W/m^2 × ster × μm)	666.09
K2 (K)	1282.71

Table 1 Details describing selected Landsat 7 ETM+ and LANDSAT 8 scenes

Landsat name	Acquisition date	Cloud cover (%)	Sun elevation	Sun azimuth
LANDSAT 7 ETM+ (LE71790342014199SG100)	18/07/2014	7.00	64.33	123.50
LANDSAT 8 (LC81790342014207LGN00)	26/07/2014	7.74	63.63	126.55

EBK automatically calculates these parameters through a process of sub-setting and simulations (Chilès and Delfiner 2012). The EBK method can handle moderately non-stationary input data estimates, and then uses many semi-variogram models rather than a single semi-variogram. EBK accounts for the error introduced by estimating the underlying semi-variogram through repeated simulations (Finzgar et al. 2014).

The method is based on 3 main steps: firstly, a semi-variogram model is estimated from the observed data set. Secondly, a new value is simulated at each of the observed data locations using the semi-variogram estimated in the previous step. Thirdly, a new semi-variogram model is estimated from the newly simulated data in the second step. By using Bayes' rule, a weight for this semi-variogram model is calculated which shows how likely the observed data can be generated from the semi-variogram. The second and third steps are repeated. This process creates a spectrum of semi-variograms. New parameters are also needed for EBK, such as a subset size which defines the number of points in each subset, an overlap factor which specifies the degree of overlap between subsets and the number of simulations, which specifies the number of semi-variograms that will be simulated for each subset.

Results

Spatial Interpolation of In Situ and Laboratory Measurement

Figures 3, 4, Supplementary Figures 1 and 2 show the EBK predictions and prediction standard error of temperature and specific conductance maps. A Semi-Variogram cloud of prediction results are presented in Supplementary Figure 3. Table 3a shows descriptive statistics of data, and Table 3b presents EBK interpolation for prediction performance (cross validation results). Prediction performances were assessed by cross validation. Cross validation enables determination of the model providing best predictions. For a model that provides accurate predictions, the standardized mean error (ME) should be close to 0, the root-mean-square error (RMS) and average standard error (AVS) should be as small as possible, and the root-mean square standardized error (RMSS) should be close to 1. According to Table 3b, the temperature of RMSS values are calculated close to 1, and the model can be considered a good fit, expect at 5 m, which could be due to instrumentation problem. RMSS is calculated over 0.8 for specific conductance, which is also a good fit for each depth. Table 4 presents the chemical composition of water and sediment samples.

The sample locations of the study are not homogenius so it was thought to make prediction standard error maps to show the locations those aren't valued well. According to the Supplementary Figures 1 and 2, the error values that can be formed of these points have been tried to be shown with these maps and it has been considered to be opened to be interpreted by everyone more correctly. Because, as seen from seismic work, the lake basin is shaped like a bowl and as the depths get closer, the coastal sections become deeper and are directed to the inner parts. As a result, the conductivity and temperature values were lost at some locations according to the geomorphology of the lake basin as it moved from the top to the deep of the lake. For this reason, the error values in the error maps showed variations with depth basis in every 5 m level changes.

The CTD results show there are probable water inputs, especially around the stream input areas and the fault area. However, interpretation could be disputed due to the small standard deviation of temperature value and specific conductivity value (Table 3a). These gradient differences could also be due to the water outputs, which could come by local flow of water between sedimentary unit and peridotite. The specific conductivity maps support the idea that they could be an effect of local flow, especially on the southeastern side of the lake. Water comes from the streams, penetrates the ground, and then it is assumed that it cannot go beyond the Peridotites, because the Peridotites are not known to be porous or permeable. Water outputs through porous medium could come only through the sedimentary unit. Water and sediment analyses also reveal the occurrence of Mg^{2+} and Fe^{2+} elements in high quantities at the bottom of the lake, which is probably because of the dissolution of peridotite. In addition, Lake Salda is located 1139 m above sea level and is broadly covered by magmatic rocks. A mountain range with an average of 1599 m altitude surrounds the catchment area, meaning the lake could also be affected by the hydrostatic head difference. Furthermore, the thermocline zone in the lake was observed at between 11 and 19 m (Supplementary Figure 4).

Remote Sensing Analyses

Landsat 7 ETM+, Landsat 8 thermal bands and in situ measurements were correlated with a regression model equation with R^2 over 0.73. According to the regression results, the surface thermal dynamic of the lake was calculated using Landsat 7 ETM+ and Landsat 8 images (Fig. 5). The temperature fluctuates between 24 and 25 °C along the shorelines. Especially, in the eastern part of the lake, the temperature is also being affected by the fault zone. At the north part of the lake, the temperature was observed at being between 12 and 20 °C. Furthermore, the

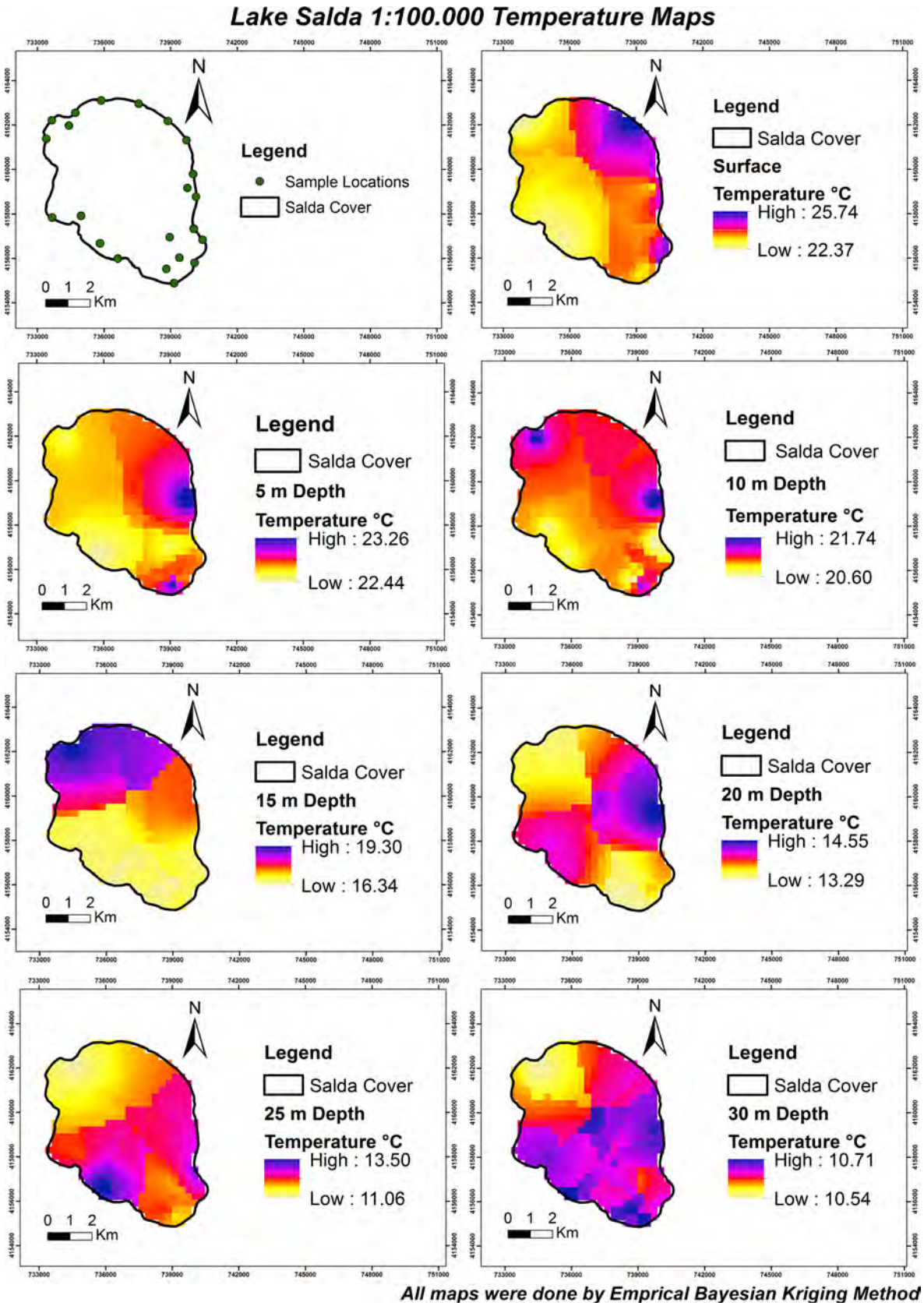

Fig. 3 Prediction map of temperature using Empirical Bayesian Kriging (EBK)

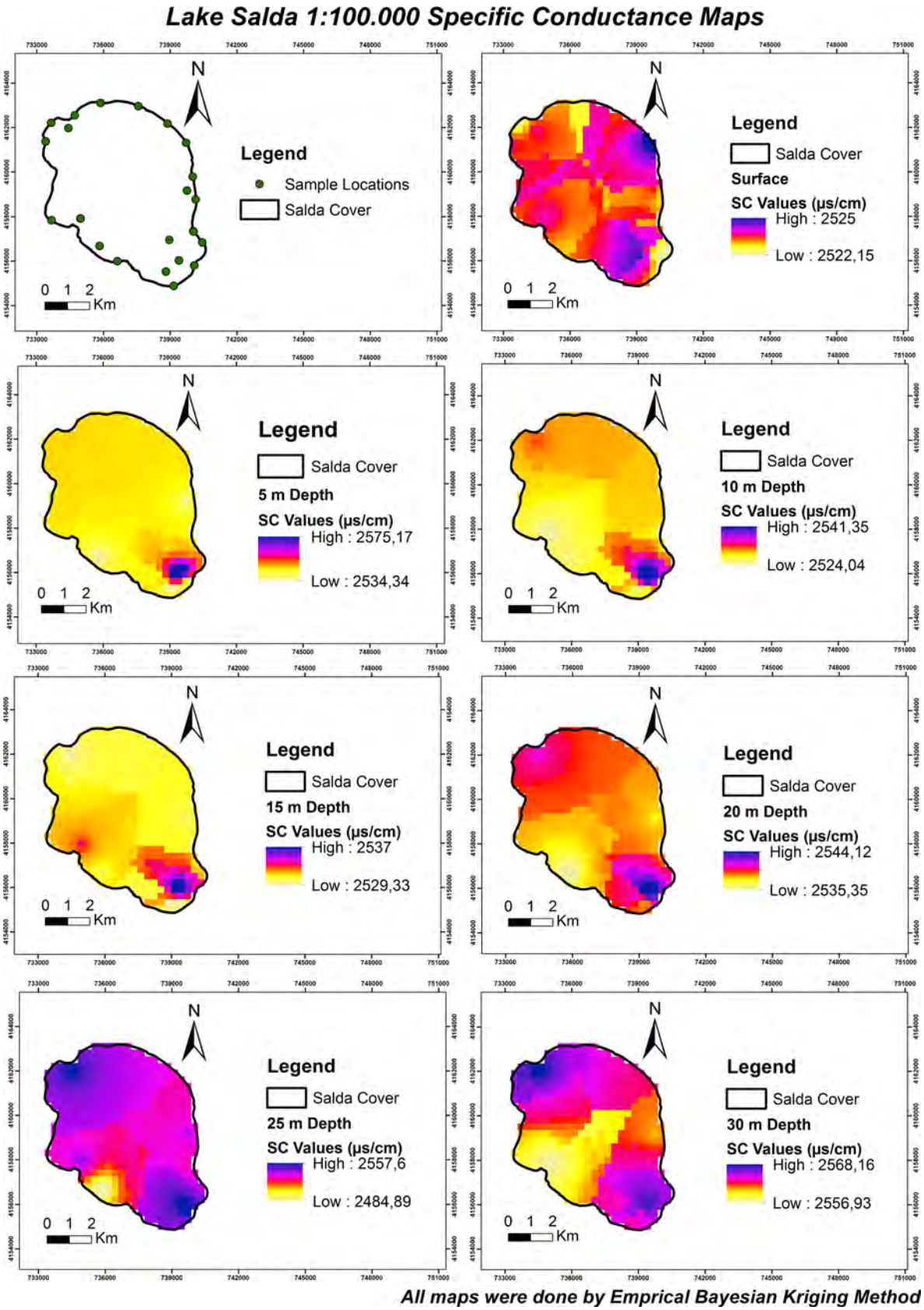

Fig. 4 Prediction map specific conductance using EBK

Table 3 (a) Descriptive statistics of in situ measurement data, (b) EBK interpolation prediction performances (cross validation results) for semi-variogram models

Depth (m)	0	5	10	15	20	25	30
(a)							
Temperature (°C)							
Minimum	22.37	22.44	21.09	16.34	13.29	11.05	10.55
Maximum	25.74	23.26	21.42	19.3	14.54	13.5	10.69
Mean	23.84	22.73	21.2	17.55	13.82	12.22	10.65
SD	0.52	0.09	0.11	0.83	0.27	0.45	0.04
Specific conductance (μs/cm)							
Minimum	2522	2534	2524	2529	2535	2485	2557
Maximum	2525	2575	2541	2538	2544	2558	2568
Mean	2524	2542	2529	2532	2539	2536	2563
SD	0.37	2.25	1.55	0.75	0.95	9.03	2.23

Depth (m)	Temperature (°C)				Specific conductance (μs/cm)			
	ME	RMS	AVS	RMSS	ME	RMS	AVS	RMSS
(b)								
0	− 0.001	0.554	0.522	0.941	0.010	37.950	47.707	0.849
5	− 0.003	1.014	0.201	0.230	0.006	28.795	31.211	0.956
10	− 0.014	0.702	0.716	0.970	0.012	26.297	28.308	0.953
15	− 0.012	0.908	0.992	0.961	− 0.008	25.687	26.973	0.968
20	− 0.114	0.486	0.560	0.882	− 0.016	12.470	13.230	0.961
25	− 0.049	0.606	0.570	1.005	− 0.035	48.454	41.321	0.892
30	− 0.030	0.458	0.488	0.941	− 0.035	12.712	14.308	0.897

ME standardized mean error, *RMS* root mean square error, *AVS* average standard error, *RMSE* root mean square standardized error

Table 4 Chemical composition of water and sediment samples

Name	Water sample					Name	Sediment sample	
	Surface and deep	Na (ppm)	Mg (ppm)	Ca (ppm)	Mg/Ca		Fe (ppb)	mg (kg)
DW01	Deep	230.75	259.54	1.95	133.26	SS01	3.59E+05	4.47E+04
DW02	Deep	230.47	241.21	1.64	146.84	SS02	1.69E+05	2.11E+04
DW03	Deep	230.55	245.80	2.51	97.79	SS04	4.57E+04	5.69E+03
DW04	Deep	161.72	203.57	1.72	118.20	SS05	1.06E+05	1.27E+04
DW05	Deep	218.07	310.75	2.12	146.76	SS06	2.07E+04	2.58E+03
DW06	Deep	221.87	284.96	1.63	175.23	SS11	1.58E+05	1.98E+04
DW07	Deep	206.64	270.75	1.92	140.80	SS13	2.32E+04	2.88E+03
DW08	Deep	225.15	257.17	1.60	160.28	G02T	1.41E+05	1.76E+04
SW01	Spring	3.67	79.16	1.23	64.28	G02B	1.79E+05	2.13E+04
SW02	River	4.14	118.63	13.36	8.88	G04T	9.18E+04	1.14E+04
SW03	River	117.92	264.48	3.32	79.63	G04B	1.15E+05	1.43E+04
TW01	Surface	228.34	259.87	2.20	118.31	G08T	1.01E+05	1.26E+04
TW02	Surface	229.58	254.03	2.42	105.09	G08B	6.65E+04	8.27E+03
TW03	Surface	78.65	119.28	1.17	101.71	G14T	1.54E+05	1.92E+04
TW04	Surface	47.06	81.72	0.80	102.23	G14B	2.07E+05	2.54E+04
TW05	Surface	231.63	253.89	2.33	108.87			
TW06	Surface	232.21	245.44	2.50	98.32			
TW07	Surface	19.28	38.62	0.38	100.76			

Table 4 (continued)

Name	Water sample					Name	Sediment sample	
	Surface and deep	Na (ppm)	Mg (ppm)	Ca (ppm)	Mg/Ca		Fe (ppb)	mg (kg)
TW08	Surface	169.26	210.62	2.35	89.66			
TW09	Surface	16.85	34.16	0.43	79.35			
TW10	Surface	223.61	239.99	2.21	108.41			
TW11	Surface	231.08	239.98	2.50	95.94			
TW12	Surface	212.58	234.27	2.43	96.26			
TW13	Surface	22.97	43.16	0.46	94.24			
TW14	Surface	230.00	237.69	0.00	–			
TW15	Surface	230.30	242.78	2.50	97.00			
TW16	Surface	231.45	253.24	1.38	183.04			
Reference material %100		204.02	252.85	507.89				
Reference material %10		20.13	36.67	51.67				
Reference material %1		2.42	5.22	7.34				

Methods for major ions = ion cromotography (IC), methods for metals = graphite furnace atomic absorption spectrometry (GF-AAS)

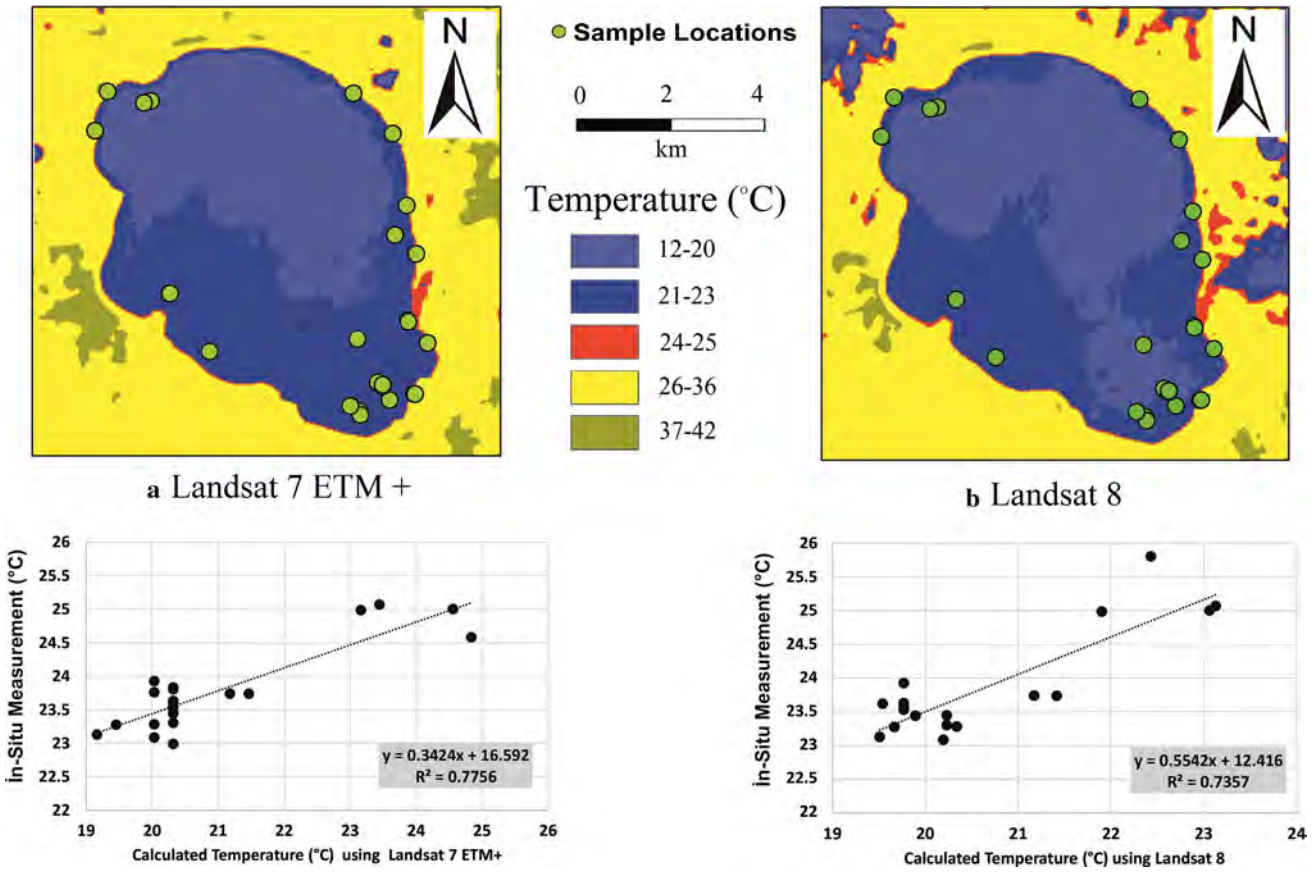

Fig. 5 Surface thermal image prediction maps and its corresponding cross-validation charts for **a** Landsat 7 ETM, **b** Landsat 8

results from the Landsat images give a more realistic pattern than interpolation results due to the lack of data in the middle of the lake.

Conceptual Model of Lake Salda

Marmaris Peridotites could be observed all around Lake Salda and cover most of the Burdur sub-basin (Fig. 2).

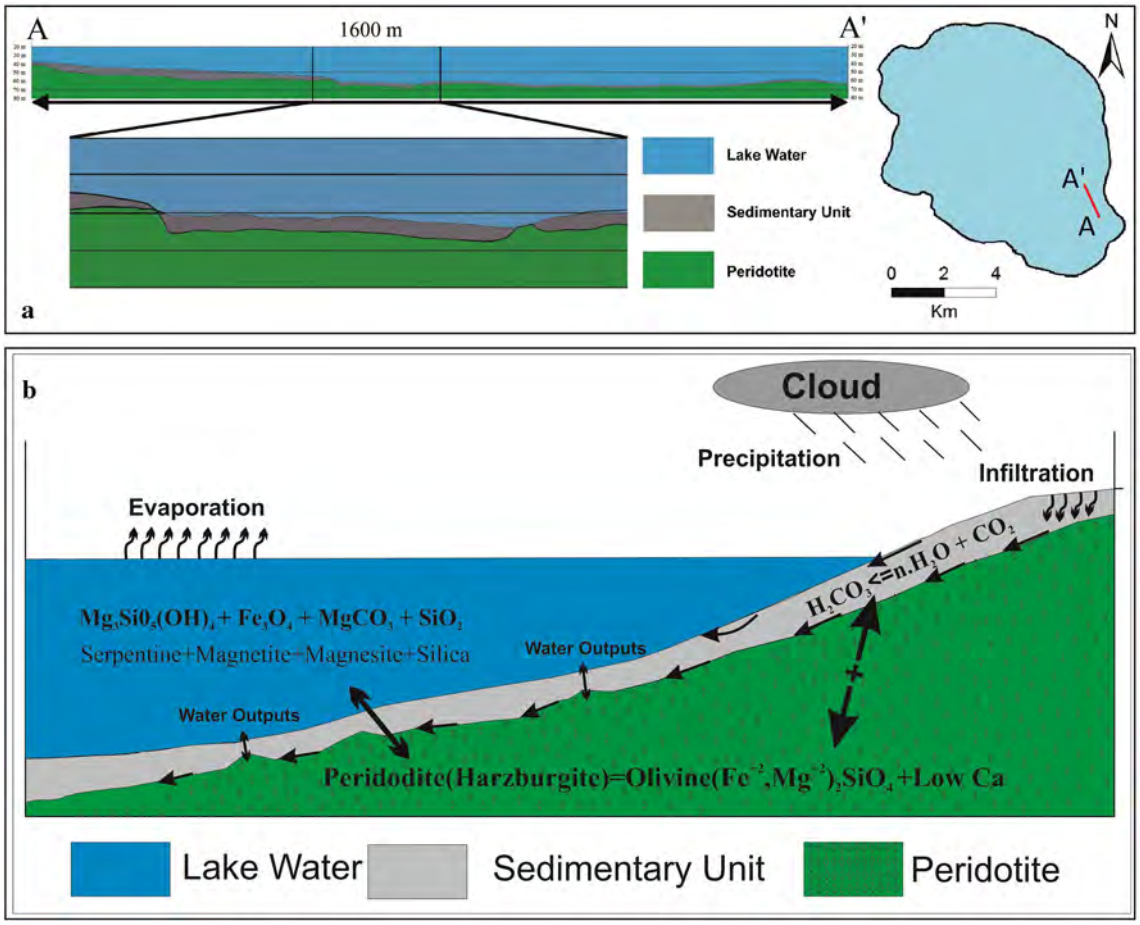

Fig. 6 **a** A–A′ cross section of the study area, **b** conceptual model of the study area

Peridotite is an igneous rock which is dense, coarse grained and consists mostly of olivine and pyroxene minerals. It is rich in magnesium and iron which is appreciable in reflecting the high proportion of magnesium rich olivine. Harzburgite, the ultramafic igneous rock, is a variety of peridotite mostly composed of olivine and low-calcium pyroxene (orthopyroxene) (Bodinier and Godard 2014) and observed harzburgites are widespread among Marmaris Peridotites (Sarp 1976). The magnesium and carbonate in the lake water were dissolved during passage through ultramafic rocks (Braithwaite and Zedef 1994). In addition, the existence of groundwater sources on the floor of the lake are possible (Kazancı et al. 2004). A seismic study also shows possible dissolution zones of peridotite at the deep profile of the lake. Regarding these results, a conceptual model of the possible recharge zones is given in Fig. 6. According to the proposed conceptual model, several peridotite dissolution points on the floor of the lake could be observed. The occurrence of abundant Fe^{2+} and Mg^{2+} elements could be viewed with the help of both water and sediment analysis records. Generally, the occurrence of Fe^{2+} metal indicates a toxic effect over a certain threshold in a lake (Tunca et al. 2013). However, Lake Salda is primarily a protected area. As a result, sources of the Fe^{2+} element could not be due to industrial pollution. According to the conceptual model, it is proposed that after precipitation, water penetrates the ground, combines with CO2 at the soil-sub-surface zone and then produces Carbonic Acid (H2CO3). Carbonic Acid interacts with peridotite, therefore, the occurrence of Mg^{2+} and Fe^{2+} is expected in the water and sediment.

Discussion

As stated by Kazancı et al. (2004), the lake is threatened by falling water levels of about 50 cm annually due to the hydraulic relationship of the lake with karstic aquifers. Karstic systems are known as the most composite systems on the Earth's surface (Bielsa et al. 2012). According to our analysis results and conceptual model, there could be peridotite dissolution zones at certain points on the lake's floor, and these could be the water input areas to the lake. Therefore, the water input to the lake could be due to the

influence of hydrostatic head differences from the surrounding mountains. In this manner, the water may come through the porous medium located on the peridotite. Furthermore, high differences in temperature or specific conductance values has not been observed. Especially, in the eastern part of the lake, a surface temperature difference has been observed. There exists a normal fault which likely causes a thermal difference outside of the lake cover.

Also, the values are decreasing in some locations according to the Emprical Bayesian Kriging maps but the values of regional differences are low. If we look at the lake as a whole, the electrical conductivity values are almost homogeneous and the temperature values fall naturally as they it gets deeper. According to these results, it is not possible to talk about a great recharge. However, especially in the range of 5–30 m depth, there may be local currents in the south eastern part of the lake in the electrical conductivity maps and in the temperature map; especially at depths of 5, 10, 20 m, there may be thought the effect of the fault to the recharge. In addition, Zehra stream is considered to be effective to the recharge for the lake at 15 m deep according to the temperature and electrical conductivity maps. In short, considering the EBK maps, it can be thought that rivers and fault lines vary in depth and are effective in lake recharge.

On the other hand, the Mg/Ca ratio, lower than 100 at one or two locations, is mainly above 100 on shore, surface and deepest points of Lake Salda. Müller et al. (1972) indicated that Mg/Ca ratio over 100 results in hydromagnesite precipitation at this high a ratio, and Russell et al. (1999) suggests Mg/Ca ratio over 100, as in our study, in part at least, is due to microbial activity (Braithwaite and Zedef 1994). So, it can be said, hyrdomagnesite precipitation still continuous in Lake Salda.

Conclusions

In this study, hydrogeochemical and physicochemical parameters were measured and analyzed to assess the evidence of recharge zones in Lake Salda. A seismic study was also carried out to determine the deep profile of the lake. In-situ measurements were taken with a CTD device and mapped using the Empirical Bayesian Kriging (EBK) interpolation method from surface to 30 m depth, at 5 m intervals. Also, a regression model was performed between in situ measurements and the thermal band of Landsat 7 ETM+ and Landsat 8 satellite images. The conceptual model was constructed according to the obtained results. The following conclusions have been determined:

According to the seismic study, water and sediment analyses, peridotite dissolution on the floor of the lake was observed by the high amounts of Mg and Fe elements. There should be water flow between peridotites and the sedimentary unit; the water inputs could likely be on the floor of the lake, the flow not being caused by the karstic springs. The flow should be through the porous medium because the peridotites are impermeable. These locations can be seen on the temperature and the specific conductance maps. The inputs are especially noticeable at the stream input locations, which are at the northern and southwestern parts are of the lake. The temperature and the specific conductance interpolation maps show the recharge zone close to the stream locations in the north and southwest.

According to the results of the thermal bands of Landsat 7 ETM+ and Landsat 8 satellite images, they show the possibility of the fault effect on the recharge zone. Temperature values showed a proper correlation with the measurements of in situ and remote sensing data ($R^2 = 0.7756$ for Landsat 7 ETM+ and $R^2 = 0.7357$ for Landsat 8). This assumption can aslo be seen in the temperature prediction map of Emprical Bayesian Kriging. It looks as navy blue at 5, 10 and 20 m depths on the eastern part of the lake, locally. Thus, it is thought that the location where the main fault is located, may be effective on the recharge of the lake.

In conclusion, Lake Salda is becoming a priority nowadays, because there are plans to construct a dam on the Düden brook. There are a number of important campaigns intended to make people understand the importance of the lake. Düden brook is merged with Karakova stream on the west, and is one of the main recharging surface waters for the lake. Although Lake Salda is one of the most important for Turkey, also the Earth, there is little data or research on it. According to this study, electrical conductance and temperature results are so close between minimum and maximum values at the same depths there is no compelling evidence for further discussion of the recharge system of the lake by groundwater. The lake is most probably fed by surface waters, so the streams have vital importance for the survival of the lake.

Acknowledgements The authors thanks for the financial support to The Scientific and Technological Research Council of Turkey (TUBITAK) "113Y408", "2210/C-2015" and Mugla Sıtkı Koçman University "BAP 15/048" projects. The authors also thank to Sena Akcer On, Kadir Eris, Eray Avcı, Illiya Bauchi Danladi for their continuing support and discussion.

References

Altınlı, İ. E. (1955). The Geology of Southern Denizli. *İstanbul University Journal of Science Faculty*, *1*(2), 1–45.

Baykal, B. B., Gönenç, I. E., Meriç, M., Tanik, A., Tunay, O., et al. (1996). An alternative approach for evaluation of lake water

quality: Lake Sapanca—A case study from Turkey. *Water Science and Technology, 34*(12), 73–81.

Bielsa, C. P., Lambán, L. J., Plata, J. L., Rubio, F. M., Soto, R., et al. (2012). Characterization of a karstic aquifer using magnetic resonance sounding and electrical resistivity tomography: A case-study of Estaña Lakes (northern Spain). *Hydrogeology Journal, 20,* 1045–1059.

Bodinier, J. L., & Godard, M. (2014). Reference module in earth systems and environmental science. *Treatise on Geochemistry, 3,* 103–167.

Bonansea, M., Rodriquez, M. C., Pinotti, L., Ferrero, S., et al. (2015). Using multi-temporal Landsat imagery and linear mixed models for assessing water quality parameters in Rio Tercero reservoir (Argentina). *Remote Sensing of Environment, 158,* 28–41.

Braithwaite, C. J. R., & Zedef, V. (1994). Living hydromagnesite stromatolites from Turkey. *Sedimentary Geology, 92,* 1–5.

Caldirak, H., Kurtulus, B., Canoglu, M. C., Tunca, E., et al. (2017). Heavy metal contamination profiles and accumulation patterns in Lake Salda, Turkey. *Fresenius Environmental Bulletin, 26*(12A), 8047–8061.

Canoğlu, M. C. (2015). *An investigation on the surface water effect in landslide susceptibility mapping: An example from Yenice (Karabük) basin*. Ph.D. thesis, Institue of Science of Hacettepe University.

Chilès, J.-P., & Delfiner, P. (2012). *Geostatistics: Modeling spatial uncertainty* (2nd ed.). Hoboken: Wiley.

Crescentini, M., Bennati, M., Tartagni, M., et al. (2012). Design of integrated and autonomous conductivity–temperature–depth (CTD) sensors. *International Journal of Electronics and Communications, 66,* 630–635.

Du, C., Ren, H., Qin, Q., Meng, J., Zhao, S., et al. (2015). A practical split-window algorithm for estimating land surface temperature from Landsat 8 data. *Remote Sensing, 7,* 647–665.

Ersoy, Ş. (1989). *Geology of the Guney Mountain and Kelebek Mountain located between Fethiye (Muğla)–Gölhisar (Burdur) area*. Ph.D. Thesis, Istanbul University Institute of Graduate Studies in Science.

ESRI. (2013). *ArcGIS desktop: Release 10.2*. Redlands, CA: Environmental Systems Research Institute.

Finzgar, N., Jez, E., Voglar, D., & Lestan, D. (2014). Spatial distribution of metal contamination before and after remediation in the Meza Valley, Slovenia. *Geoderma*, *217–218*, 135–143.

Kazancı, N., Sönmez, G., Dügel, M., et al. (2004). On the limnology of Salda Lake, A large and deep soda lake in southwestern Turkey: Future management proposals. *Aquatic Conservation: Marine and Freshwater Ecosystems, 14,* 151–162.

Kocaefe, S., & Ataman, G. (1976). Seismotectonic events in Anatolia-1: Investigation of the area within the Antalya–Fethiye–Denizli triangle. *Bulletin for Earth Sciences, 1*(1), 55–70.

Krivoruchko, K. (2011). *Spatial statistical data analysis for GIS users* (p. 928). Redlands, CA: ESRI Press.

Markham, B. L., & Barker, J. K. (1985). Spectral characteristics of the LANDSAT Thematic Mapper sensors. *International Journal of Remote Sensing, 6,* 697–716.

MTA. (2010). 1/:100000 Scale Geological Maps of Turkey. Report No.: 16 Second Edition Publication of Mineral Research and Exploration Institute of Turkey.

Müller, G., Irion, G., Förstner, U., et al. (1972). Formation and diagenesis of inorganic Ca–Mg carbonates in the lacustrine environment. *The Science of Nature, 59,* 158–164.

Poisson, A. (1977). *Geological Research in Western Taurides (Turkey)*. Ph.D. Thesis, Paris-Sud (Orsay) State University.

Russell, M. J., Ingham, J. K., Zedef, V., Maktav, D., Sunar, F., Hall, A. J., et al. (1999). Search for signs of ancient life on Mars: Expectations from hydromagnesite microbialites, Salda Lake, Turkey. *Geological Society of London Journal, 156,* 869–888.

Sarp, H. (1976). *Etude geoloqique et petropraphique du Cortege Ophiolitique de la Region Situee au Nord-Ouest de Yeşilova (Burdur-Turkey)*. Thesis, University of Geneve.

Thuizat, R., Whitechurch, H., Montigny, R., & Juteau, T. (1981). K-Ar dating of some infraophiolitic metamorphic soles from the Eastern Mediterranean. *New Evidence for oceanic thrusting before obduction, Earth and Planetary Science Letters*, *52*, 302–310.

Trescott, A., & Park, M. H. (2014). Remote sensing models using Landsat satellite data to monitor algal blooms in Lake Champlain. *Water Science and Technology, 67,* 1113–1120.

Tunca, E., Ucuncu, E., Kurtuluş, B., Ozkanc, A. D., Atasagun, S., et al. (2013). Accumulation effects and trends of some heavy metal (Al, Cu, Fe, Ni, Zn) and a metalloid (As) in the freshwater crayfish. *Ecology and Chemistry, 29,* 754–769.

Vlassova, L., Perez-Cabello, F., Nieto, H., Martín, P., Riaño, D., de la Riva, J., et al. (2014). Assessment of methods for land surface temperature retrieval from Landsat-5 TM images applicable to multiscale tree-grass ecosystem modeling. *Remote Sensing, 6,* 4345–4368.

Wetzel, R. G. (2001). *Limnology. Lake and river ecosystems*. San Diego: Elsevier Academic Press.